JACS
JOURNAL OF THE AMERICAN CHEMICAL SOCIETY

COMMUNICATION

pubs.acs.org/JACS

Electronic Packing Frustration in Complex Intermetallic Structures: The Role of Chemical Pressure in Ca_2Ag_7

Daniel C. Fredrickson

Department of Chemistry, University of Wisconsin—Madison, 1101 University Avenue, Madison, Wisconsin 53706, United States

Supporting Information

ABSTRACT: The assignment of distinct roles to electronics and sterics has a long history in our rationalization of chemical phenomena. Exploratory synthesis in the field of intermetallic compounds challenges this dichotomy with a growing list of phases whose structural chemistry points to an interplay between atomic size effects and orbital interactions. In this paper, we begin with a simple model for how this interdependence may arise in the dense atomic packing of intermetallics: correlations between interatomic distances lead to the inability of a phase to optimize bonds without simultaneously shortening electronically under-supported contacts, a conflict we term *electronic packing frustration* (EPF). An anticipated consequence of this frustration is the emergence of chemical pressures (CPs) acting on the affected atoms. We develop a theoretical method based on DFT-calibrated μ_2-Hückel calculations for probing these CP effects. Applying this method to the Ca_2Ag_7 structure, a variant of the $CaCu_5$ type with defect planes, reveals its formation is EPF-driven. The defect planes resolve severe CPs surrounding the Ca atoms in a hypothetical $CaCu_5$-type $CaAg_5$ phase. CP analysis also points to a rationale for these results in terms of a CP analogue of the pressure-distance paradox and predicts that the impetus for defect plane insertion is tunable via variations in the electron count.

For all of their differences, tantalizing parallels exist between the chemistries of molecules and intermetallic phases. One example is the distinction between electronic and steric effects. This distinction is particularly central to our conceptual understanding of metals, as the consideration of neither electronic states nor atomic sizes alone provides a fully satisfying depiction of the metallic state. The conductivity and delocalized bonding in metals is vividly captured by the modern view of their electronic structure as derived from Bloch wave functions or crystal orbitals delocalized over the entire crystal.[1] However, this view does not directly address the rich structural variety intermetallics exhibit at the more local level of individual coordination polyhedra. These geometrical features are better embraced with a concept closely connected to sterics, that of close packing of spheres with definite radii.[2] As the electronic and sphere-packing perspectives highlight different aspects of metals, they are often viewed as describing different factors governing stability.

Exploratory synthesis, however, is challenging this dichotomy with a growing number of phases whose structures are governed by interactions between electronic and size effects.[3] In this Communication, we will describe a theoretical approach to integrating these contributions to stability, focusing on their interdependence at the outset. In doing so we will see a simple model emerge that can express the results of DFT calculations in a predictive language suggestive of new synthetic endeavors.

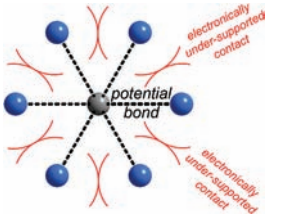

Figure 1. Schematic illustration of electronic packing frustration.

Let us begin with a simple picture of how atomic size and electronic interactions may be coupled in intermetallics. The structures of these phases usually exhibit dense atomic packing, with coordination numbers (CNs) of 14, 16, 18, or even higher being common.[2e] With such high CNs, contact distances become difficult to adjust independently of each other, i.e., strong correlations occur among the interatomic distances. One might wonder then to what extent the observed distances reflect ideal bond lengths and to what extent they represent a compromise between competing interactions. The answer to this question will largely depend on how quantum mechanics distributes bonding electron density throughout the structure (Figure 1). When optimization of bonding contacts requires shortening neighboring contacts with little electronic support, a tension arises. We refer to this conflict between the dictates of electronics and the realities of atomic size as *electronic packing frustration* (EPF).

Over the course of this paper, we will build on the concept of EPF using as a model system a phase for which empirical evidence hints that such frustration plays a role: Ca_2Ag_7. It crystallizes in a variant of the $CaCu_5$ type (exemplified in Figure 2 by Ca_2Ag_7's closest strontium analogue, $SrAg_5$[4]) in which layers of Ag atoms are deleted periodically along the *c*-axis, resulting in the more complex monoclinic Yb_2Ag_7 structure type (Figure 2c).[5]

The stability of this superstructure relative to the simpler, more common $CaCu_5$ type appears to be connected to both atomic size and electron count. While Ca_2Ag_7 is the closest known approximation to a $CaCu_5$-type phase in the Ca−Ag system,[6] this superstructure gives way to its $CaCu_5$-type parent structure in many related systems. $CaCu_5$-type phases are observed for $SrAg_5$[4,7] and $CaCu_5$[8] in which Ca or Ag of Ca_2Ag_7 is substituted with elements of different atomic size, and $CaPd_5$[9] in which substitution of Ag with Pd leaves the ratio of atomic sizes largely unchanged but lowers the electron count by five per formula unit.

Received: May 9, 2011
Published: May 28, 2011

ACS Publications © 2011 American Chemical Society

dx.doi.org/10.1021/ja203944a | *J. Am. Chem. Soc.* 2011, 133, 10070–10073

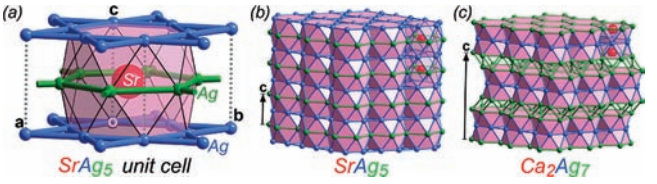

Figure 2. Comparison of the $SrAg_5$ and Ca_2Ag_7 crystal structures. Panel (a) focuses on a single $SrAg_5$ unit cell, while panel (b) zooms out to show multiple cells for comparison with Ca_2Ag_7 in panel (c).

This dependence of the Ca_2Ag_7 structure on both atomic size and electron count suggests a role for EPF in its stability.

How might we find clearer indications that EPF is involved in the formation of the Ca_2Ag_7 structure? In structures with severe EPF, the interatomic distances are restrained from reaching their ideal lengths. One consequence of this could be the emergence of local pressures acting on the affected atoms. The notion of such local pressures induced by the constraints of a crystal lattice has a long history under the term *chemical pressure* (CP).[10] In our analysis of Ca_2Ag_7, we will see that this concept, when expressed in the language of orbital interactions, unifies the roles of atomic size and electronics in intermetallic phases.

In the next paragraphs, we will develop a simple theoretical approach to analyzing and visualizing CP distributions in crystal structures. The basis of this approach is classic Hückel theory.[11] The simple Hückel method has a number of advantages for investigating EPF. First is its potential for accuracy, with the proper parametrization. In Figure 3a,b, we compare the band structures calculated for Ca_2Ag_7's simpler Sr counterpart, $SrAg_5$, with GGA-DFT[12] and with the Hückel method[13] using parameters refined against the DFT result.[14] While some differences are apparent, there is a close correspondence between these band structures: the root-mean-squared deviation in the energy levels up to 1 eV above the Fermi energy (E_F) is only 0.04 eV.

A second convenient feature of the Hückel method is the transparent connection it affords between geometry and electronic structure. This connection is made explicit by the Method of Moments:[15] the moments of the electronic density of states (DOS) can be written both as functions of the DOS curve,

$$\mu_n = \int_{-\infty}^{\infty} E^n \,\mathrm{DOS}(E)\,\mathrm{d}E$$

and as functions of the structure via sums of products of Hamiltonian matrix elements (H_{ij}),[15b]

$$\mu_n = \sum_{i_1}\sum_{i_2}\cdots\sum_{i_n} H_{i_1 i_2} H_{i_2 i_3}\ldots H_{i_{n-1} i_n}$$

The link between structure and the DOS is completed by the ability to reconstruct a DOS curve from its moments using any of a variety of moments inversion schemes.

A third advantage of the Hückel method is that, when supplemented with a short-range interatomic repulsion potential, it can reproduce the expected distance dependence of bonding interactions. A convenient formulation for this is given by the μ_2-Hückel model.[16] Here the repulsion energy of the system is approximated as being proportional to the second moment (μ_2) of the DOS, leading to the total energy $E_{\mu_2\text{-Hückel}} = \gamma\mu_2 + E_{\text{Hückel}}$, where γ is a proportionality constant (usually chosen to reproduce the equilibrium volume of a structure), and $E_{\text{Hückel}}$ is the sum of the energies of the electrons from a simple Hückel calculation. Despite its simplicity, the μ_2-Hückel method works; it has been successfully applied in elucidating structural trends in systems ranging from Hume–Rothery phases[17] to stacked organic π-radical cations.[18]

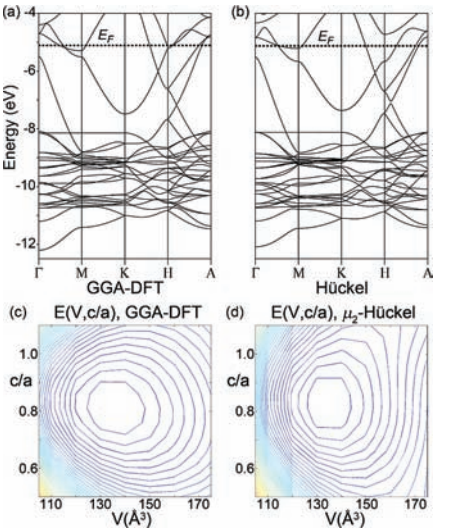

Figure 3. Validation of a DFT-calibrated Hückel model for $SrAg_5$. (a,b) Band structures of $SrAg_5$ calculated with (a) GGA-DFT and (b) a best-fit Hückel model. (c,d) Contour plots of the $SrAg_5$ total energy as a function of unit cell volume (V) and c/a ratio calculated using (c) GGA-DFT and (d) the μ_2-Hückel method.

The use of the μ_2-Hückel method allows us to reproduce not only the distribution of electronic energy levels as calculated with GGA-DFT but also the energetics for distortions of the unit cell. This is illustrated in Figure 3c,d with contour maps of the total energy of $SrAg_5$ as functions of its unit cell's volume (V) and the c/a ratio calculated using GGA-DFT and a best-fit μ_2-Hückel model.[19] The match between the two levels of theory here is not as quantitative as in the band structures, but there are key similarities. The two plots agree on the location of the minimum as well as the scale of the energetics involved (in both, the contours are drawn at intervals of 0.2 eV).

When the DFT results are translated into a μ_2-Hückel model, as illustrated for $SrAg_5$, the CPs can be analyzed in a simple way. Because $\mu_2 = \Sigma_i\Sigma_j H_{ij}H_{ji} = \Sigma_i\Sigma_j H_{ij}^2$, the total energy can be expressed as a sum of onsite and pairwise interaction terms:[16]

$$E_{\mu_2\text{-Hückel}} = \gamma\mu_2 + E_{\text{Hückel}} = \sum_i\sum_j(\gamma H_{ij}^2 + (\sum_n o_n c_{n,i}^* c_{n,j})H_{ij})$$

where $c_{n,j}$ is the coefficient of atomic orbital j in crystal orbital n, and o_n is the occupancy of that crystal orbital. This expression allows us to similarly decompose the pressure of a phase ($P = -\partial E/\partial V$) into an average over individual pairwise interactions:

$$P = -\frac{\partial E}{\partial V} = -\sum_i\sum_j \frac{\partial}{\partial V}(\gamma H_{ij}^2 + (\sum_n o_n c_{n,i}^* c_{n,j})H_{ij}) = \frac{1}{N_{\text{orb}}}\sum_i\sum_j p_{ij}$$

where N_{orb} is the number of orbitals in the crystal, and p_{ij} is the pressure arising from the interaction between atomic orbitals i and j ($i = j$ terms are zero). In other words, within the μ_2-Hückel method, the total pressure can be expressed as an average of CP contributions arising from individual bonding interactions. At the energy-minimized volume, the total pressure is zero, and the above equation amounts to resolving the static equilibrium into a sum of competing terms.

In the left panel of Figure 4a, we show what this type of analysis can tell us about $SrAg_5$. Here, we add up all the CP contributions acting on each atom and represent these net CPs as spheres. The radius of each sphere is proportional to the magnitude of the net CP experienced by the corresponding atom, while the sphere color gives the sign of the CP—black for negative, white for positive. This convention is based on an astronomical analogy: an

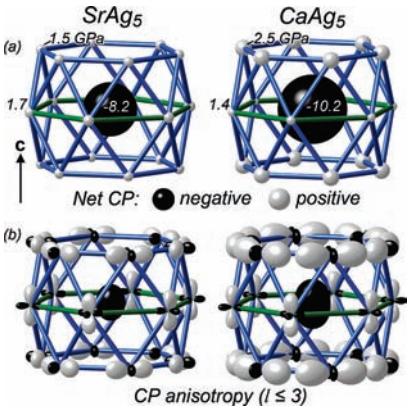

Figure 4. μ_2-Hückel chemical pressure (CP) analysis of $SrAg_5$ (left) and a hypothetical $CaCu_5$-type $CaAg_5$ phase (right). (a) Net CP values for the Sr or Ca atom and its neighboring Ag atoms. CP values are plotted as spheres, with the color indicating the sign of the CP (black for negative, white for positive) and the radius giving the magnitude. (b) Distributions of the CP contributions around each atom projected onto low-order spherical harmonics ($l \leq 3$).

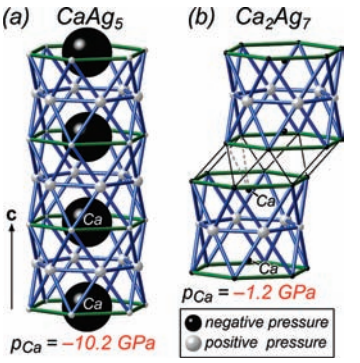

Figure 5. μ_2-Hückel chemical pressure (CP) analysis of (a) a hypothetical $CaCu_5$-type $CaAg_5$ phase and (b) Ca_2Ag_7. Net CP values are plotted with spheres, following the conventions of Figure 4. p_{Ca} gives values for the net CP acting on the Ca atoms.

atom with a black sphere is pulling its neighbors toward it like a black hole, while an atom plotted with a white sphere is pushing out on its surroundings like a white-hot star radiates.

From this plot, it is clear that substantial CPs are present in the structure. The Sr atom is represented by a large black sphere, corresponding to a net CP value of −8.2 GPa. This is balanced by the CP values of the Ag atoms, which appear as small white spheres describing net CP values of 1.5 or 1.7 GPa.

We can see how these CP values result from Sr−Ag and Ag−Ag interactions by investigating the spatial distribution of the CP terms about each atom. A visual way of exploring this is to project these CP contributions onto low-order spherical harmonics centered on each atom, and then graph the weighed sum of these functions as a representation of the angular distribution of the local pressures acting upon the atom. Such CP anisotropy functions are displayed for $SrAg_5$ in Figure 4b. Each atom is overlaid with a radial surface consisting of lobes in white and black. The radial extent of the surface along any given direction is proportional to the magnitude of the CP along that direction, while the color indicates the sign as described above.

Here, the black sphere of the Sr atom now appears slightly stretched along *c*, but the CP distribution appears to be negative along all directions, indicating that the contacts of the Sr to its Ag neighbors are longer than ideal. Bonding here could be enhanced through contraction of the Sr coordination polyhedron. The Ag atom CP anisotropy surfaces explain why such contraction does not occur. The Ag atoms all have white lobes with components along the Ag−Ag contacts in blue; these contacts are already too short. Compressing the structure to optimize the Sr−Ag interactions would further strain overly short Ag−Ag contacts.

From these results, we can understand why no Ca version of this phase is observed. Our CP analysis of $SrAg_5$ reveals that Sr is already too small for its electronic context in this structure. On replacing Sr with the smaller Ca, the need for contraction around the Ca to obtain reasonable Ca−Ag distances would exacerbate the Ag−Ag strain. A μ_2-Hückel CP analysis of a hypothetical $CaCu_5$-type $CaAg_5$ phase (using a structure geometrically optimized with GGA-DFT, and Hückel parameters refined against the DFT results as described in the Supporting Information) confirms this (Figure 4a, right): the net CP computed for the Ca atom increases from the −8.2 GPa calculated for Sr in $SrAg_5$ to −10.2 GPa. The increased EPF around the Ca is also evident in the shape of its CP anisotropy surface (Figure 4b, right). The surface is now more profoundly elongated along *c*, indicating that the distances to the Ag atoms in the planes above and below are particularly strained.

These CP results for $CaAg_5$ anticipate the observed Ca_2Ag_7 structure. One way of soothing some of the overstretched Ca−Ag contacts along *c* would be to move the Ca atom out of the plane, shortening the contacts to the Ag atoms either above or below. Doing so, of course, would add further strain to the Ca−Ag contacts on the opposite side. However, the situation changes drastically if such a motion of the Ca atom is coupled with the insertion of a defect plane on the opposite side, as in Ca_2Ag_7 (Figure 5). The defect plane supports the Ca atom's motion out of the honeycomb layer by positioning two Ag atoms behind it at a close distance (3.24 Å vs the average Ca−Ag distance of 3.52 Å for $CaAg_5$), as indicated with dashed gray lines in Figure 5b.

Comparison of the CP values calculated for $CaAg_5$ and Ca_2Ag_7 confirms this picture, as shown in Figure 5. In Figure 5a, the Ca atoms of $CaAg_5$ appear again as large black spheres, indicating high negative CP values of −10.2 GPa. In Figure 5b, we move to Ca_2Ag_7. Here the large black spheres on the Ca have largely vanished, with small black remnants corresponding to a CP value of only −1.2 GPa. The transition from $CaAg_5$ to Ca_2Ag_7 has thus largely relieved the large negative Ca CP.

Another way of looking at these results is found by comparing the Ca coordination environments in the hypothetical $CaAg_5$ and the observed Ca_2Ag_7 phases. During the transition from $CaAg_5$ to Ca_2Ag_7, the CN of the Ca by Ag changes from 18 to 14, with the average Ca−Ag distance decreasing from 3.52 to 3.31 Å (see Figure S1 in the Supporting Information).[20] This parallel decrease in both the CN and the contact lengths in response to negative pressure mirrors a classic trend in pressure-induced phase transitions, the *pressure-distance paradox*:[21] upon going from a low-pressure to a high-pressure phase, CNs generally increase. The increased number of bonds to each atom means that individual bonds are weaker, and the interatomic distances are consequently longer. Bond lengths increase, despite the higher pressure. On going from high-pressure to low-pressure phases, the trend reverses. CNs decrease, while bond lengths shrink.

The transition between $CaAg_5$ and Ca_2Ag_7 can be understood in a similar language when physical pressure is replaced with chemical pressure. In $CaAg_5$, the Ca atoms experience negative CP. In response, the Ca CN decreases, with shorter Ca−Ag distances arising.

In short, defect plane insertion into the $CaCu_5$ type to produce the Ca_2Ag_7 structure can be viewed as a CP-induced structural transition.

So far, we have seen that the μ_2-Hückel CP analysis can explain the nonexistence of $CaAg_5$ and the origin of the Ca_2Ag_7 structure. The simplicity of the method also allows us to make predictions about how the driving force for defect plane insertion in the $CaCu_5$ type depends on variables controllable in a synthetic experiment, such as the valence electron concentration. Increasing the valence electron count by one per formula unit exacerbates the negative net CP of the Ca in $CaAg_5$ from −10.2 to −13.4 GPa. Decreasing the valence electron count by the same amount, on the other hand, soothes the Ca net CP from −10.2 to −7.1 GPa. The impetus for the insertion of defect planes is then predicted to decrease if Ag were to be partially substituted with an element with fewer valence electrons but similar size, such as Pd. Substitution with a similarly sized element with more valence electrons, such as Cd, would increase the driving force. Such predictions are consistent with the observations that $CaPd_5$ adopts the $CaCu_5$ type, while the Ca−Cd phase diagram exhibits a $Gd_{14}Ag_{51}$-type phase in which 20-atom fragments of the $CaCu_5$ type occur.[22] These results also hint that other variants of the $CaCu_5$ type between these extremes may be synthesizable by partial substitution of Ag with Cd or Pd.

Here, we have considered one mechanism by which complex structures may be stabilized in intermetallics, electronic packing frustration, and have pursued the implications of this mechanism through a theoretical analysis of the Ca_2Ag_7 structure. We saw through μ_2-Hückel CP analysis that such frustration indeed underlies the formation of this phase. The $CaCu_5$-type $CaAg_5$ phase that might be expected in the Ca−Ag system is calculated to have large negative CP values around the Ca atoms. Insertion of planar defects to create the Ca_2Ag_7 structure brings relief by providing the Ca sites with a smaller, tighter coordination environment. This can be rationalized by extending the pressure-distance paradox to CP-induced phenomena.

This analysis has relied upon the transparency of the μ_2-Hückel method as well as its ability to reproduce the results of higher-level calculations. However, the CP analysis can be extended beyond semiempirical methods. The key feature of μ_2-Hückel that our CP approach uses is the ability to decompose the total energy into a sum over a spatial distribution of contributions to the energy, in this case bonds and onsite terms. In principle, the total DFT electronic energy could be similarly decomposed, this time as an integral over the energy density distributed over the unit cell. A DFT−CP distribution could then be obtained from the derivative of this energy density with respect to the unit cell volume. We will present our efforts to realize such a DFT-based CP analysis, as well as an exploration of the generality of the CP analogue of the pressure-distance paradox, in future articles on CP as a driving force for structural complexity in intermetallics.

■ ASSOCIATED CONTENT

Supporting Information. Appendix with theoretical procedures and Hückel parameters; Figure S1. This material is available free of charge via the Internet at http://pubs.acs.org.

■ AUTHOR INFORMATION

Corresponding Author
danny@chem.wisc.edu

■ ACKNOWLEDGMENT

I am grateful to Patrick Sims for testing the μ_2-Hückel CP method on other intermetallic systems and for engaging discussions. I am also thankful for the financial support of the University of Wisconsin (through start-up funds) and the DOE Office of Science Early Career Program (DE-SC0003947) through the Office of Basic Energy Sciences.

■ REFERENCES

(1) (a) Bloch, F. *Z. Phys.* **1928**, *52*, 555.(b) Hoffmann, R. *Solids and surfaces: a chemist's view of bonding in extended structures*; VCH Publishers: New York, 1988.

(2) (a) Hume-Rothery, W.; Raynor, G. V. *The structure of metals and alloys*, 4th ed.; Institute of Metals: London, 1962. (b) Laves, F. *Theory Alloy Phases* **1956**, 124. (c) Frank, F. C.; Kasper, J. S. *Acta Crystallogr.* **1958**, *11*, 184. (d) Frank, F. C.; Kasper, J. S. *Acta Crystallogr.* **1959**, *12*, 483.(e) Pearson, W. B. *The crystal chemistry and physics of metals and alloys*; Wiley-Interscience: New York, 1972. (f) Simon, A. *Angew. Chem.* **1983**, *95*, 94.

(3) (a) Amerioun, S.; Häussermann, U. *Inorg. Chem.* **2003**, *42*, 7782. (b) Mozharivskyj, Y.; Tsokol, A. O.; Miller, G. J. *Z. Kristallogr.* **2006**, *221*, 493. (c) Li, B.; Corbett, J. D. *Inorg. Chem.* **2007**, *46*, 8812. (d) Xia, S.-Q.; Bobev, S. *J. Am. Chem. Soc.* **2007**, *129*, 10011.

(4) Palenzona, A. *Atti Accad. Naz. Lincei, Cl. Sci. Fis., Mat. Nat., Rend.* **1967**, *42*, 504.

(5) (a) Cordier, G.; Henseleit, R. *Z. Kristallogr.* **1991**, *194*, 146. (b) Snyder, G. J.; Simon, A. *J. Alloys Compd.* **1995**, *223*, 65.

(6) Baren, M. R. In *Binary Alloy Phase Diagrams*; Massalski, T. B. O. H., Subramanian, P. R., Kacprzak, L., Eds.; ASM International: Materials Park, OH, 1990; p 20.

(7) The Sr−Ag phase diagram also exhibits a phase with the composition $SrAg_4$, whose structure is unknown. See ref 6, p 97. The composition $SrAg_4$ is consistent with a defect variant of the $CaCu_5$ type, similar to the Ca_2Ag_7 structure but with a lower frequency of defect planes.

(8) Haucke, W. *Z. Anorg. Allg. Chem.* **1940**, *244*, 17.

(9) Mejbar, J.; Notin, M. *Scr. Metall. Mater.* **1990**, *24*, 1697.

(10) The CP concept is most often used when describing how elemental substitutions aimed at varying atomic sizes influence physical properties. For examples of the application of this concept to structural distortions, see: (a) DiMasi, E.; Aronson, M. C.; Mansfield, J. F.; Foran, B.; Lee, S. *Phys. Rev. B* **1995**, *52*, 14516. (b) Kim, S.-J.; Ponou, S.; Faessler, T. F. *Inorg. Chem.* **2008**, *47*, 3594.

(11) (a) Hückel, E. *Z. Phys.* **1931**, *70*, 204. (b) Hückel, E. *Z. Phys.* **1932**, *76*, 628.

(12) (a) GGA-DFT calculations were performed with the VASP package using projected augmented wave potentials. See Supporting Information for details. (b) Kresse, G.; Furthmueller, J. *Phys. Rev. B* **1996**, *54*, 11169. (c) Kresse, G.; Furthmuller, J. *Comput. Mater. Sci.* **1996**, *6*, 15. (d) Bloechl, P. E. *Phys. Rev. B* **1994**, *50*, 17953. (e) Kresse, G.; Joubert, D. *Phys. Rev. B* **1999**, *59*, 1758.

(13) Hückel calculations were carried out with YAeHMOP: Landrum, G. A. *YAeHMOP: Yet Another extended Hückel Molecular Orbital Package*, Version 3.0; http://sourceforge.net/projects/yaehmop/.

(14) For examples of quantitatively refining extended Hückel parameters against higher-level calculations, see: (a) Berger, R. F.; Walters, P. L.; Lee, S.; Hoffmann, R. *Chem. Rev.* **2011**DOI: 10.1021/cr1001222. (b) Cerdá, J.; Soria, F. *Phys. Rev. B* **2000**, *61*, 7965.

(15) (a) Gaspard, J. P.; Cyrot-Lackmann, F. *J. Phys. C* **1973**, *6*, 3077. (b) Burdett, J. K.; Lee, S. *J. Am. Chem. Soc.* **1985**, *107*, 3050.

(16) Lee, S. *Annu. Rev. Phys. Chem.* **1996**, *47*, 397.

(17) Hoistad, L. M.; Lee, S. *J. Am. Chem. Soc.* **1991**, *113*, 8216.

(18) Devic, T.; Yuan, M.; Adams, J.; Fredrickson, D. C.; Lee, S.; Venkataraman, D. *J. Am. Chem. Soc.* **2005**, *127*, 14616.

(19) Comparisons of plots of the total energy as a function of V and c/a calculated for simpler structures with DFT and the μ_2-Hückel method are described in the following: Todorov, E.; Evans, M.; Lee, S.; Rousseau, R. *Chem. Eur. J.* **2001**, *7*, 2652.

(20) For maximal consistency in the comparison of hypothetical and observed crystal structures, all interatomic distances refer to structures optimized with GGA-DFT (see the Supporting Information).

(21) (a) Kleber, W. *Kris. Technik* **1967**, *2*, 13.(b) Müller, U. *Inorganic structural chemistry*, 2nd ed.; Wiley: Chichester, 2007.

(22) (a) Bailey, D. M.; Kline, G. R. *Acta Crystallogr. B* **1971**, *27*, 650. (b) Bruzzone, G. *Gazz. Chim. Ital.* **1972**, *102*, 234.